The Astrophysical Journal, 778:102 (12pp), 2013 December 1 doi:10.1088/0004-637X/778/2/102

AN INTENSELY STAR-FORMING GALAXY AT $z \sim 7$ WITH LOW DUST AND METAL CONTENT REVEALED BY DEEP ALMA AND *HST* OBSERVATIONS

Masami Ouchi[1,2], Richard Ellis[3], Yoshiaki Ono[1], Kouichiro Nakanishi[4,5], Kotaro Kohno[6,7], Rieko Momose[1], Yasutaka Kurono[5], M. L. N. Ashby[8], Kazuhiro Shimasaku[7,9], S. P. Willner[8], G. G. Fazio[8], Yoichi Tamura[6], and Daisuke Iono[10]

[1] Institute for Cosmic Ray Research, The University of Tokyo, 5-1-5 Kashiwanoha, Kashiwa, Chiba 277-8582, Japan; ouchims@icrr.u-tokyo.ac.jp
[2] Kavli Institute for the Physics and Mathematics of the Universe (WPI), The University of Tokyo, 5-1-5 Kashiwanoha, Kashiwa, Chiba 277-8583, Japan
[3] Department of Astrophysics, California Institute of Technology, MS 249-17, Pasadena, CA 91125, USA
[4] The Graduate University for Advanced Studies (SOKENDAI), 2-21-1 Osawa, Mitaka, Tokyo 181-8588, Japan
[5] Joint ALMA Observatory, Alonso de Cordova 3107, Vitacura, Santiago 763-0355, Chile
[6] Institute of Astronomy, University of Tokyo, 2-21-1 Osawa, Mitaka, Tokyo 181-0015, Japan
[7] Research Center for the Early Universe (WPI), University of Tokyo, 7-3-1 Hongo, Bunkyo, Tokyo 113-0033, Japan
[8] Harvard-Smithsonian Center for Astrophysics, 60 Garden Street, Cambridge, MA 02138, USA
[9] Department of Astronomy, Graduate School of Science, The University of Tokyo, 7-3-1 Hongo, Bunkyo-ku, Tokyo 113-0033, Japan
[10] National Astronomical Observatory of Japan, 2-21-1 Osawa, Mitaka, Tokyo 181-8588, Japan
Received 2013 June 15; accepted 2013 August 23; published 2013 November 11

ABSTRACT

We report deep ALMA observations complemented by associated *Hubble Space Telescope* (*HST*) imaging for a luminous ($m_{\rm UV} = 25$) galaxy, "Himiko," at a redshift of $z = 6.595$. The galaxy is remarkable for its high star formation rate, 100 $M_\odot$ yr^{-1}, which has been securely estimated from our deep *HST* and *Spitzer* photometry, and the absence of any evidence for strong active galactic nucleus activity or gravitational lensing magnification. Our ALMA observations probe an order of magnitude deeper than previous IRAM observations, yet fail to detect a 1.2 mm dust continuum, indicating a flux of $<52\,\mu$Jy, which is comparable to or weaker than that of local dwarf irregulars with much lower star formation rates. We likewise provide a strong upper limit for the flux of [C II] 158 μm, $L_{\rm [C\,II]} < 5.4 \times 10^7\ L_\odot$, which is a diagnostic of the hot interstellar gas that is often described as a valuable probe for early galaxies. In fact, our observations indicate that Himiko lies off the local $L_{\rm [C\,II]}$–star formation rate scaling relation by a factor of more than 30. Both aspects of our ALMA observations suggest that Himiko is a unique object with a very low dust content and perhaps nearly primordial interstellar gas. Our *HST* images provide unique insight into the morphology of this remarkable source, highlighting an extremely blue core of activity and two less extreme associated clumps. Himiko is undergoing a triple major merger event whose extensive ionized nebula of Lyα emitting gas, discovered in our earlier work with Subaru, is powered by star formation and the dense circumgalactic gas. We are likely witnessing an early massive galaxy during a key period of its mass assembly close to the end of the reionization era.

Key words: cosmology: observations – galaxies: formation – galaxies: high-redshift

1. INTRODUCTION

Much progress has been achieved in recent years in charting the abundance and integrated properties of the earliest galaxies beyond a redshift of $z \simeq 6$ selected via optical and near-infrared (NIR) photometry (e.g., Bouwens et al. 2010a; McLure et al. 2010, 2012; Castellano et al. 2010; Ouchi et al. 2010; Ellis et al. 2013; Schenker et al. 2012). The emerging picture indicates that the redshift period $6 \lesssim z \lesssim 10$ was a formative one in the assembly history of normal galaxies. Sources at $z \simeq 7$–8 show moderately blue ultraviolet continua, which may be consistent with young, metal-poor stellar populations with a star-formation rate (SFR) of 1–10 $M_\odot$ yr^{-1} (e.g., Bouwens et al. 2010b; Finkelstein et al. 2010; Schaerer & de Barros 2010; Dunlop et al. 2012). Their small physical sizes ($\simeq$0.7 kpc; Oesch et al. 2010; Ono et al. 2012a) and modest stellar masses (10^8–10^9 $M_\odot$; Labbé et al. 2010) suggest that they quickly merge into larger, more luminous systems. The abundance of sub-luminous, small galaxies at high redshift also indicates that significant merging occurred at early times, given that the faint-end slope of the UV luminosity function changes from a steep $\alpha \simeq -1.9$ at $z = 7$–8 (Schenker et al. 2012; McLure et al. 2012) to $\alpha \simeq -1.7$ at $z = 2$–3 (e.g., Reddy & Steidel 2009).

In practice, it is hard to decipher the physical processes that govern the early assembly of galaxies from integrated properties alone. We therefore seek to complement statistical measurements such as SFRs and stellar masses with detailed evidence from well-studied individual examples. Likewise, our understanding of early cosmic history may be incomplete given that so much is currently deduced from optical and NIR data alone (Robertson et al. 2013). Although optical and NIR-selected sources at high redshift suggest that they contain little or no dust (Bouwens et al. 2012; Dunlop et al. 2013), this may be a selection bias. Star formation obscured by dust cannot be quantified without identifying cold dust emission. Furthermore, the gas phase metallicity remains a key measurement for understanding early systems, most notably in locating the highly prized pristine "first generation" systems unpolluted by supernova enrichment. Neither optical nor NIR facilities can currently address this important question since the diagnostic metal lines used at lower redshift, such as [O II] $\lambda\lambda$3726, 3729 and [O III] $\lambda\lambda$5007, 4959, cannot be measured beyond $z \simeq 5$ until the launch of the *James Web Space Telescope*.

For this reason, state of the art sub-millimeter facilities such as the Atacama Large Millimeter Array (ALMA) offer enormous promise. First, they can quantify the possible bias in our current "optical" view of early galaxy formation by detecting the hidden cold dust in high redshift galaxies. Second, the CO/[C II] 158 μm features prominent in star-forming regions in the local universe offer a valuable tracer of metallicity at

early times. Thus far, neither the cold dust continuum nor these low-ionization tracers of metallicity have been observed beyond $z \sim 6$ (Vieira et al. 2013; Capak et al. 2011; Riechers et al. 2010; Coppin et al. 2010). Although a few QSOs have been observed at sub-millimeter wavelengths to $z = 6.4$–7.1 (Maiolino et al. 2005; Iono et al. 2006; Walter et al. 2009; Venemans et al. 2012; Willott et al. 2013; Wang et al. 2013), the presence of a powerful active galactic nucleus (AGN) undoubtedly complicates any understanding of the physical conditions in their host galaxies.

Detecting these important diagnostic signals of dust and metallicity from typical $z \simeq 7$ galaxies is clearly a major observational challenge. Only upper limits on [C II] and sub-millimeter continuum fluxes have been presented so far for the abundant population of Lyman break galaxies (LBGs) and Lyα emitters (LAEs) at $z \sim 7$. These limits have come from deep exposures with the sub-millimeter Common-User Bolometer Array (SCUBA; Holland et al. 1999) facility on the James Clerk Maxwell telescope and Plateau de Bure interferometric observations (e.g., Ouchi et al. 2009b; Walter et al. 2012; Kanekar et al. 2013). Very recently, one $z = 6.34$ source was studied in this way following a comprehensive search for red objects in the *Herschel* HerMES blank field survey at 50–500 μm (Riechers et al. 2013). This source, HFLS3, has very strong far-infrared (FIR) continuum emission and prominent molecular/low-ionization lines. Its SFR, inferred from its FIR luminosity, is extremely high, 2900 $M_\odot$ yr^{-1}. Clearly, we need to understand the context of this remarkable object by observing other sources at a similar redshift.

The present work is concerned with undertaking such a study for an extraordinarily luminous star-forming galaxy which will hopefully complement the study of HFLS3 by Riechers et al. (2013). Ouchi et al. (2009b) reported the discovery of a star-forming galaxy at $z = 6.595$, "Himiko,"[11] with a *Spitzer*/IRAC counterpart. This source was identified from an extensive 1 deg^2 optical survey for $z = 6.6$ galaxies in the UKIDSS/UDS field conducted with the Subaru telescope. The redshift was subsequently confirmed spectroscopically using Keck/DEIMOS. The unique features of this remarkable source are evident when compared to the total sample of 207 galaxies at $z = 6.6$ found in the panoramic Subaru survey. Not only is Himiko by far the most luminous example ($M_{\rm UV} = 25$; $L({\rm Ly}\alpha) = 4 \times 10^{43}$ erg s^{-1}), but it is spatially extended in Lyα emission, whose largest isophotal area is 5.22 arcsec^2, corresponding to a linear extent of over 17 kpc. The lower limit, SFR $> 34\,M_\odot$ yr^{-1}, is placed on the SFR of Himiko by the spectral energy distribution (SED) fitting analysis with the early photometric measurements and the stellar-synthesis and nebular-emission models (Ouchi et al. 2009b). Due to the large uncertainties of photometric measurements, Ouchi et al. (2009b) cannot constrain $E(B-V)$, and provide only the lower limit of SFR with $E(B-V) \geqslant 0$.

The present paper is concerned with the analysis of uniquely deep ALMA and *Hubble Space Telescope* (*HST*) observations of this remarkable source. Given its intense luminosity and high SFR, we presume that it is being observed at a special time in its assembly history. We seek to use the cold dust continuum and [C II] measures from ALMA to understand its dust content and gas phase metallicity. Likewise, the matched resolution of *HST* will allow us to address its morphologic nature. Fortunately, one of the *HST* intermediate band filters closely matches the intense Lyα emission observed for this source with Subaru. Ultimately, we seek to understand the physical source of the energy that powers the extensive Lyα nebula.

The plan of the paper is as follows. We describe our ALMA and *HST* observations in Section 2, and present the detailed properties such as dust-continuum and metal-line emission, morphology, and stellar population in Section 3. We discuss the nature of this object in Section 4 and summarize our findings in Section 5. Throughout this paper, magnitudes are in the AB system. We adopt $(h, \Omega_m, \Omega_\Lambda, n_s, \sigma_8) = (0.7, 0.3, 0.7, 1.0, 0.8)$.

2. OBSERVATIONS AND MEASUREMENTS

2.1. ALMA

To understand whether obscured star-formation is an important issue and to determine the metallicity of Himiko, a key source at high redshift, we carried out deep ALMA Band 6 observations in 2012 July 15, 18, 28, and 31 with a 16 12 m antenna array under the extended configuration of 36–400 m baseline. The precipitable water vapor ranged from 0.7 to 1.6 mm during the observations. We targeted Himiko's [C II] rest-frame 1900.54 GHz (157.74 μm), which is redshifted to 250.24 GHz (1.198 mm) at a redshift of $z_{{\rm Ly}\alpha} = 6.595$. Since we expect a brighter dust continuum at a higher frequency in the 1.2 mm regime, we extended our upper sideband (USB) to the high-frequency side. Thus, we targeted the [C II] line with the lowest spectral window (among four spectral windows) in the lower sideband (LSB) and set the central frequency of the four spectral windows to be 250.24 and 252.11 GHz in LSB, and 265.90 and 267.78 GHz in USB with a bandwidth of 1875 MHz. The two spectral windows and each sideband contiguously cover the frequency ranges. The total on-source integration time was 3.17 hr. We used 3c454.3 and J0423−013 for bandpass calibrators and J0217+017 for a phase calibrator. The absolute flux scale was established by observations of Neptune and Callisto. Our data were reduced with the Common Astronomy Software Applications package. We rebin our data to a resolution of 166 MHz (200 km^{-1}). The FWHM beam size of the final image is $0\farcs82 \times 0\farcs58$ with a position angle of 79°.5. The 1σ noise of the continuum image is $\sigma_{\rm cont} = 17.4\,\mu$Jy beam^{-1} over the total bandwidth of 19.417 GHz, whose 7.5 GHz is sampled. The 1σ noise of the [C II] line image is $\sigma_{\rm line} = 83.3\,\mu$Jy beam^{-1} at 250.239 GHz over a channel width of 200 km^{-1}.

Further details of the ALMA observations and sensitivities are summarized in Table 1.

We averaged fluxes over the two spectral windows of LSB (249.30–253.05 GHz or 1.203–1.185 mm) and USB (264.96–268.71 GHz or 1.131–1.116 mm) in the range of frequency free from the [C II] line. Figure 1 presents the resulting ALMA continuum data at the 259.01 GHz frequency (or 1.167 mm in wavelength) with a 1σ sensitivity of 17.4 μJy beam^{-1}. There is a $\sim 2\sigma$ flux peak in the beam size at the position of Himiko. However, there are a series of negative pixels nearby that correspond to the 2σ–3σ level per beam. We conclude therefore that Himiko remains undetected in the 1.2 mm continuum with a 3σ upper limit of $<52.1\,\mu$Jy beam^{-1}. We note that this sensitivity is two and one order(s) of magnitudes better than those previously obtained by deep SCUBA/SHADES and IRAM/PdBI observations (Ouchi et al. 2009b; Walter et al. 2012). This clearly indicates that Himiko has very weak millimeter emission. Table 1 summarizes the flux upper limits for the continuum and [C II] line derived from our ALMA data.

[11] See Ouchi et al. (2009b) for the meaning of this name.

Table 1
ALMA Observations and Sensitivities

$\nu_{\rm cont}$ (GHz) (1)	$\nu_{\rm line}$ (GHz) (2)	$\sigma_{\rm cont}$ (μJy beam^{-1}) (3)	$\sigma_{\rm line}$ (μJy beam^{-1}) (4)	$f_{\rm cont}$ (μJy) (5)	$f_{\rm line}$ (μJy) (6)	$L_{\rm FIR}$ (10^{10} $L_\odot$) (7)	$L_{\rm [C\,II]}$ (10^7 $L_\odot$) (8)
259.007	250.239	17.4	83.3	<52.1	<250.0	<8.0	<5.4

Notes. Columns: (1) and (2) central frequencies of continuum and [C II] line observations that correspond to 1.16 and 1.20 mm, respectively. (3) and (4) 1σ sensitivities for continuum and [C II] line in a unit of μJy beam^{-1}. The continuum sensitivity given in the total bandwidth for the continuum measurement is 19.417 GHz or 86.894 μm, which is a sum of four spectral windows (see text). The line sensitivity is defined with a channel width of 200 km^{-1}. (5) and (6) 3σ upper limits of continuum and [C II] line in a unit of μJy. (7) and (8) 3σ upper limits of far-infrared continuum luminosity (8–1000 μm) and [C II] line luminosity in a unit of 10^{10} and 10^7 solar luminosities, respectively. We estimate 3σ upper limits of far-infrared continuum luminosities at 40–500 μm and 42.5–122.5 μm to be $<7.36 \times 10^{10}$ and $<6.09 \times 10^{10}$ $L_\odot$, respectively. These far-infrared luminosities are estimated with the assumptions of the graybody, $\beta_{\rm d} = 1.5$, and a dust temperature of $T_d = 40$ K.

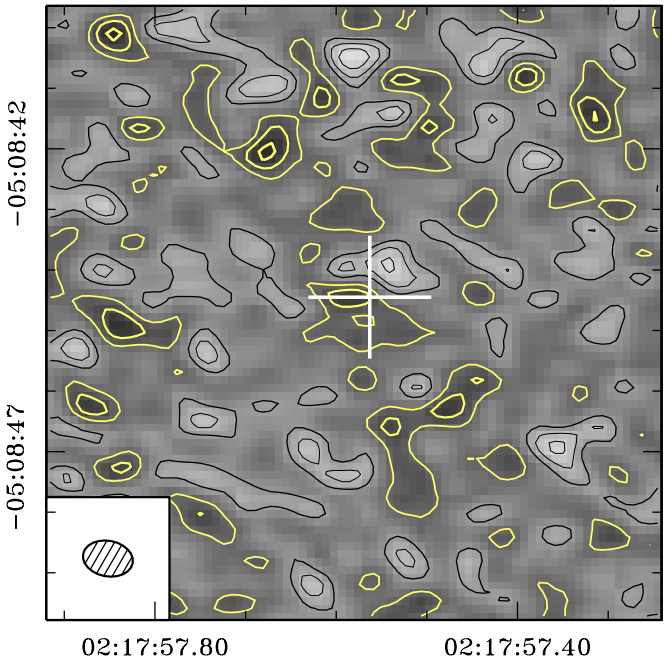

Figure 1. ALMA continuum data for Himiko at 259 GHz (1.16 mm). The gray scale indicates the intensity at each position where darker regions imply higher intensities. The black contours denote -3σ, -2σ, and -1σ levels, while yellow contours show $+1\sigma$, $+2\sigma$, and $+3\sigma$ significance levels where the 1σ flux corresponds to 17.4 μJy beam^{-1}. The white cross indicates the position of Himiko. The ellipse in the lower corner denotes the beam size.

Figure 2 shows the ALMA [C II] velocity channel maps for Himiko. We searched for a signal of [C II] over 600 km^{-1} around the frequency corresponding to $z_{\rm Ly\alpha} = 6.595$. In Figure 2, there are noise peaks barely reaching the 3σ level in 0 km s^{-1} and -200 km s^{-1} that are slightly north and south of Himiko's optical center position, respectively. However, neither of these sources is a reliable counterpart of Himiko. Although the ALMA data reach a 1σ noise of 83.3 μJy beam^{-1}, no [C II] line is detected. The corresponding 3σ upper limit for [C II] is 250.0 μJy in a channel width of 200 km s^{-1}. The associated luminosity limit is $<5.4 \times 10^7$ $L_\odot$.

2.2. *HST*

The primary goal of the associated *HST* observations of Himiko is related to the morphological nature of this remarkable source. We carried out deep *HST*/WFC3-IR broad-band (J_{125} and H_{160})[12] and medium-band ($F098M$) observations for Himiko. The two broad-band filters J_{125} and H_{160} measure the rest-frame UV continuum fluxes and are free from contamination from Lyα emission, thus maximizing the amount of information on the stellar content for SED fitting (Section 3.3). The intermediate-band filter of $F098M$ fortuitously includes the spectroscopically confirmed Lyα line of Himiko at 9233 Å (Ouchi et al. 2009b) with a system throughput of 40%, which is close to the peak throughput of this filter (∼45%). Thus, the $F098M$ image is ideal for mapping the distribution of Lyα emitting gas.

Our observations were conducted in 2010 September 9, 12, 15–16, 18, and 26 with an orientation of 275°. Some observations were partially lost because *HST* went into "safe mode" on 2010 September 9, 22:30 during the execution of one visit. The total integration times for usable imaging data are 15670.5, 13245.5, 18064.6 s for $F098M$, J_{125}, and H_{160}, respectively. The various WFC3 images were reduced with the WFC3 and MULTIDRIZZLE packages on PyRAF. To optimize our analyses, in the multidrizzle processing we chose a final_pixfrac = 0.5 and pixel scale of 0.″05132. We degraded images of $F098M$ and J_{125} to match the point spread functions (PSFs) of these images with that of H_{160}, which has the largest size among the *HST* images. We ensured that the final WFC3 images have a matched PSF size of 0.″19 FWHM.

Figure 3 presents a color composite *HST* UV-continuum image of Himiko as well as a large ionized Lyα cloud identified by the Subaru observations (Ouchi et al. 2009b). This image reveals that the system comprises three bright clumps of starlight surrounded by a vast Lyα nebula $\gtrsim$17 kpc across. We denote the three clumps as A, B, and C. Figure 4 shows the *HST*, Subaru, and *Spitzer* images separately. The $F098M$ image in Figure 4 detects only marginal extended Lyα emission, because of the shallower surface brightness limit of the 2.4 m *HST* compared to the 8 m Subaru telescope. Nevertheless, we have found a possible bright extended component at position D in Figure 4. We perform 0.″4 diameter aperture photometry for clumps A–C and location D as well as 2″ diameter aperture photometry, which we adopt as the total magnitude of the system. Tables 2 and 3 summarize the photometric properties. It should be noted that Himiko is not only identified as an LAE, but also would be regarded as an LBG or "dropout" galaxy. Using the optical photometry of Ouchi et al. (2009b; see also Table 3), we find no blue continuum fluxes for filters *B*

[12] J_{125} and H_{160} are referred to as $F125W$ and $F160W$, respectively.

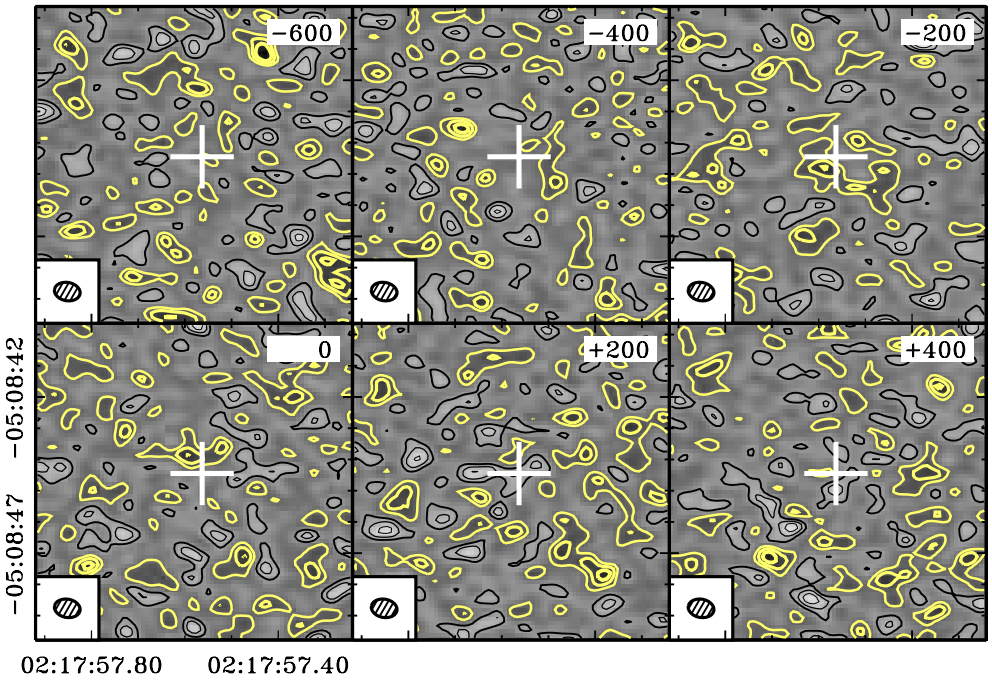

Figure 2. As Figure 1, but for [C II] velocity channel maps of Himiko whose 1σ intensity is 83.3 μJy beam^{-1}. The six panels present maps of 200 km^{-1} width at central velocities of −600, −400, −200, 0, +200, and +400 km s^{-1} from the top left to the bottom right. 0 km s^{-1} corresponds to [C II] emission at the redshift $z_{\mathrm{Ly}\alpha} = 6.595$, i.e., 250.24 GHz (1.198 mm).

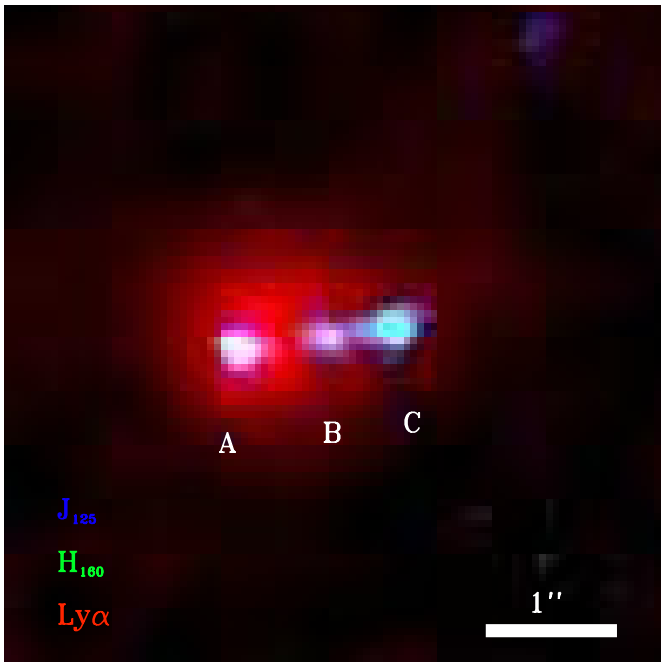

Figure 3. Color composite image of Himiko. Blue and green represent *HST*/WFC3 continua of J_{125} and H_{160}, respectively. Red indicates Lyα emission resolved with sub-arcsec-seeing Subaru observations. The Lyα emission image comprises the Subaru $NB921$ narrowband data with a subtraction of the continuum estimated from the seeing-matched *HST*/WFC3 data. The three continuum clumps are labeled A, B, and C.

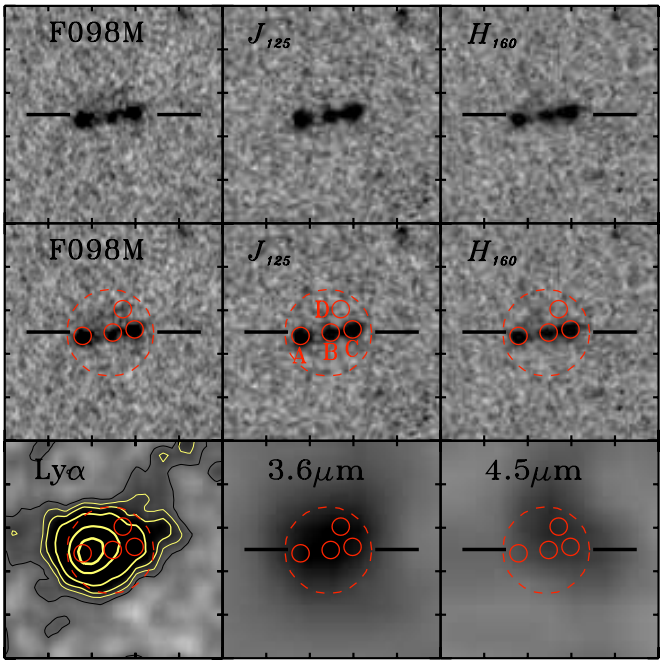

Figure 4. *HST*, Subaru, and *Spitzer* images of Himiko; north is up and east is to the left. Each panel presents 5″ × 5″ images at $F098M$, J_{125}, and H_{160} bands from *HST*/WFC3, 3.6 μm and 4.5 μm bands from *Spitzer* SEDS. The Lyα image is a Subaru $NB921$ image continuum subtracted using J_{125} and includes intensity contours. The Subaru image has a PSF size of 0.″8. The solid red circles indicate the positions of 0.″4 diameter apertures for Clumps A, B, C, and D photometry in the *HST* images (see Section 2.2 for details), while the dashed red circles denote 2″ diameter apertures used for the defining the total magnitudes.

through i' up to the relevant detection limits of 28–29 mag. The very red color of $i' - z' > 2.1$ meets typical dropout selection criteria (e.g., Bouwens et al. 2011). Because the z'-band photometry includes the Lyα emission line and an Lyα-continuum break, we can also estimate the continuum break color using our *HST* photometry of J_{125} and H_{160} and the optical i-band photometry. Assuming the continuum spectrum is flat ($f_\nu = $ const.), we obtain a continuum break color $i' - J_{125} > 3.0$ or $i' - H_{160} > 3.0$, further supporting Himiko's classification as an LBG. Importantly, these classifications also apply to clumps A–C, ruling out the possibility that some could be foreground sources.

Table 2
Properties of the Subcomponents

Component	x(pix)	y(pix)	NB (mag)	J_{125} (mag)	H_{160} (mag)	β	L(Lyα) (10^{42} erg s^{-1})	EW$_0$ (Å)	SFR(UV) ($M_\odot$ yr^{-1})	SFR(Lyα) ($M_\odot$ yr^{-1})
(1)	(2)	(3)	(4)	(5)	(6)	(7)	(8)	(9)	(10)	(11)
Total[a]	2815.4	2790.4	23.55 ± 0.05	24.99 ± 0.08	24.99 ± 0.10	-2.00 ± 0.57	38.4 ± 1.5	78^{+8}_{-6}	30 ± 2	35 ± 1
(F098M)	...	...	(24.84 ± 0.08)	...	...	...	(30.5 ± 15.6)	(61^{+28}_{-23})	...	(28 ± 14)
A(clump)	2803.0	2789.0	26.36 ± 0.04	26.54 ± 0.04	26.73 ± 0.06	-2.84 ± 0.32	8.1 ± 1.9	68^{+14}_{-13}	7 ± 0	7 ± 2
B(clump)	2816.5	2790.5	27.19 ± 0.09	27.03 ± 0.07	27.04 ± 0.08	-2.04 ± 0.47	0.2 ± 1.9	3^{20}_{-18}	5 ± 0	0 ± 2
C(clump)	2826.3	2791.9	26.57 ± 0.05	26.43 ± 0.04	26.48 ± 0.05	-2.22 ± 0.28	0.8 ± 1.9	6^{+12}_{-10}	8 ± 0	1 ± 2
D	2821	2801	28.47 ± 0.29	>28.86	>28.70	...	>1.7	>123	<1	>2

Notes. Columns: (1) Name of the component. (2) and (3) Positions in pixels. (4)–(6) Aperture magnitudes in NB, J_{125}, and H_{160}. NB indicates a narrow/intermediate band magnitude determined with $F098M$ for all lines except in Total(NB921). The upper limit corresponds to a 3σ limit. (7) UV-continuum slope. (8) Lyα luminosity. (9) Rest-frame apparent equivalent width of Lyα emission line in Å. (10) Star-formation rate estimated from the UV magnitude. (11) Star-formation rate estimated from the UV magnitude.
[a] The *NB* magnitude corresponds to $NB921$. The quantities of Columns 8, 9, and 11 are estimated from $NB921$ photometry.

Table 3
Total Magnitudes and Fluxes of Himiko

Band	Mag/Flux(Total)[a]
B[b]	>28.7
V[b]	>28.2
R[b]	>28.1
i'[b]	>28.0
z'[b]	25.86 ± 0.20
$NB921$[b]	23.55 ± 0.05
$F098M$	24.84 ± 0.08
J_{125}	24.99 ± 0.08
H_{160}	24.99 ± 0.10
J[c]	25.03 ± 0.25
H[c]	26.67 ± 2.21
K[c]	24.77 ± 0.29
$m(3.6\,\mu\mathrm{m})$	23.69 ± 0.09
$m(4.5\,\mu\mathrm{m})$	24.28 ± 0.19
$m(5.8\,\mu\mathrm{m})$[b]	>22.0
$m(8.0\,\mu\mathrm{m})$[b]	>21.8
$m(24\,\mu\mathrm{m})$[b]	>19.8
$S(1.2\,\mathrm{mm})$	$<52.1\,\mu$Jy[d]
f([C II])	$<250.0\,\mu$Jy[d]

Notes.
[a] In units of AB magnitudes, if not specified. The upper limits are 2σ and 3σ magnitudes in $BVRi'$ and 5.8–24 μm bands, respectively.
[b] Measurements obtained in Ouchi et al. (2009b). The continuum magnitudes from B through z' are defined with a $2''$ diameter aperture photometry that matches to the photometry of the total magnitudes of NIR bands.
[c] Total magnitudes from UKIDSS/UDS DR8 data that are estimated with a $2''$ diameter aperture photometry and the aperture correction in the same manner as Ono et al. (2010b).
[d] Three sigma upper limits derived with our ALMA data.

The UV continuum magnitudes of clumps A–C range from 26.4 to 27.0 mag in J_{125} and H_{160}. Each clump has a UV luminosity corresponding to the characteristic luminosity L^* of a $z \sim 7$ galaxy, $m = 26.8$ mag (Ouchi et al. 2009a; Bouwens et al. 2011). Moreover, the variation in luminosity across the components is small; there is no single dominant point source in this system, confirming earlier deductions that the system does not contain an active nucleus.

The $F098M$ image shows that Lyα emission is not uniformly distributed across the three clumps. Clump A shows intense Lyα emission with a rest-frame equivalent width (EW$_0$) of 68^{+14}_{-13} Å, placing it in the category of a LAE, whereas clumps B and C have emission more typical of LBGs with a rest-frame Lyα equivalent width (EW$_0$) less than 20 Å given the measurement uncertainties.

In summary, the *HST* and Subaru data indicate that Himiko is a triple L^* galaxy system comprising one LAE and two LBGs surrounded by an extensive 17 kpc diffuse Lyα halo. Importantly, from the above morphological studies, we can easily eliminate the possibility that Himiko is gravitationally lensed by a foreground concentration. Ouchi et al. (2009a) have already made a strong case against lensing given that Keck spectroscopy revealed a velocity gradient of 60 km s^{-1} across the system. We can further reject this supposition given that there are clear asymmetries in the outermost images (one has strong Lyα emission and the other does not).

2.3. Spitzer

Although *Spitzer* cannot match the resolution of the above morphological data, we use the very deep *Spitzer*/IRAC SEDS data reaching 26 mag at the 3σ level (Ashby et al. 2013) to investigate the counterpart of the overall Himiko system at the 3.6 μm and 4.5 μm bands. To improve the relative astrometric accuracy, we have realigned the SEDS images to the *HST* images, referring to bright stellar objects commonly detected in the *Spitzer* and *HST* images. The relative astrometric errors are estimated to be $\simeq 0\farcs1$ rms. We obtain total magnitudes for the *Spitzer*/IRAC images from a $3''$ diameter aperture and use an aperture correction given in Yan et al. (2005). The total magnitudes are 23.69 ± 0.09 mag and 24.28 ± 0.19 mag at the 3.6 μm and 4.5 μm bands, respectively. Because the *Spitzer*/IRAC 5.8 μm and 8.0 μm and *Spitzer*/MIPS 24 μm band images are not available in the SEDS data set, we use the relatively shallow *Spitzer*/SpUDS (PI: J. Dunlop, 2007) photometry measurements presented in Ouchi et al. (2009b). Table 3 summarizes these total magnitudes and fluxes.

3. RESULTS

Ouchi et al. (2009b) found that Himiko has a high SFR ($>34\,M_\odot$ yr^{-1}) and derived a moderately high stellar mass (0.5–$5.0 \times 10^{10}\,M_\odot$) from the Subaru photometry and shallow

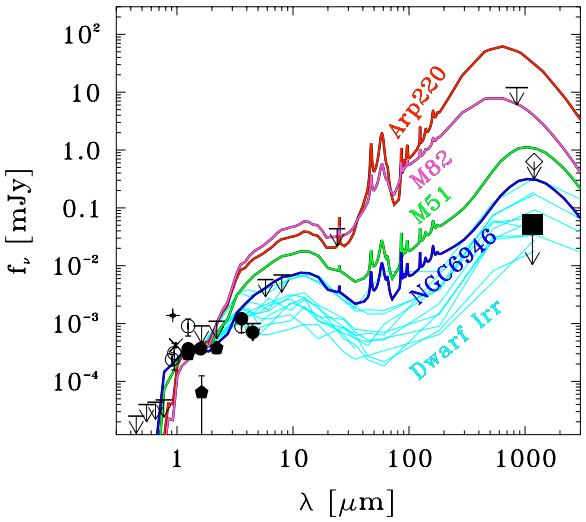

Figure 5. Optical to far-infrared SED of Himiko in the observed frame. The filled square shows the upper limit from our deep ALMA Band 6 observations and the filled circles represent photometry from *HST*/WFC3 J_{125} and H_{160} photometry and *Spitzer* SEDS 3.6 and 4.5 μm. The filled pentagons indicate the UKIDSS-UDS DR8 *J*, *H*, and *K* photometry. The cross and plus symbols denote *HST*/WFC3 *F*098*M* and Suprime-Cam *NB*921 photometry that includes Lyα emission and the Gunn–Peterson trough in their bandpasses. The open circles and arrows are data points and the upper limits taken from Ouchi et al. (2009b). The open diamond with an arrow shows the upper limit from the IRAM observations (Walter et al. 2012). The red, magenta, green, and blue lines represent the SEDs of local galaxies, Arp220, M82, M51, and NGC 6946 (Silva et al. 1998), respectively, redshifted to $z = 6.595$. SEDs of local dwarf irregular galaxies similarly redshifted are presented with cyan lines (Dale et al. 2007). All local galaxy SEDs are normalized in the rest-frame UV, where Himiko's SED is reliably determined.

Spitzer/SpUDS data. Here, we attempt to improve upon these estimates and for the first time secure information on dust content and inter-stellar medium (ISM) metallicity.

3.1. Far Infrared SED

We investigate obscured star-formation and dust properties of Himiko from its FIR SED using the newly available ALMA 1.2 mm continuum data. The SED from the optical to millimeter wavelengths is shown in Figure 5, together with that of various local starburst templates. The figure demonstrates that Himiko's millimeter flux is significantly weaker than that of dusty starbursts in the local universe such as Arp220 and M82, as well as the spiral galaxy NGC 6946; it is more comparable to those of dwarf galaxies of much lower mass. Similarly, Himiko's rest-frame optical flux derived from the *Spitzer*/IRAC 3.6 and 4.5 μm photometry is significantly weaker than that of dusty starbursts and spiral galaxies. Given its intense rest-frame UV luminosity and moderately high stellar mass, Himiko's dust emission and evolved stellar flux are remarkably weak. Both properties imply a low extinction and a relatively young stellar age (Section 3.3). In this sense, Himiko may be similar to many luminous $z \sim 3$ LBGs whose cold-dust continuum emission is also comparable to unreddened local starburst galaxies (Ouchi et al. 1999).

We can estimate a FIR luminosity of Himiko from our 1.2 mm continuum limit. Assuming an optically thin graybody of modified blackbody radiation with a dust emissivity power-law spectral index of $\beta_{\rm d} = 1.5$ and a dust temperature of $T_d = 40$ K (Eales et al. 1989; Klaas et al. 1997), we obtain a 3σ upper limit of $L_{\rm FIR} < 8.0 \times 10^{10}\ L_\odot$ integrated over 8–1000 μm. We also estimate 3σ upper limits of $<7.4\times10^{10}$ and $<6.1\times10^{10}\ L_\odot$ at 40–500 μm and 42.5–122.5 μm, respectively. Note that these upper limits depend upon the assumed dust temperature and $\beta_{\rm d}$. For $T_d = 25$ K and $T_d = 60$ K, the 3σ upper limit luminosities in 8–1000 μm are $<2.7 \times 10^{10}$ and $<3.0 \times 10^{11}\ L_\odot$, respectively. Similarly, for $\beta_{\rm d} = 0$ and $\beta_{\rm d} = 2$, the 3σ upper limit luminosities in 8–1000 μm are $<3.5 \times 10^{10}$ and $<1.2 \times 10^{11}\ L_\odot$, respectively.

The preceding upper luminosity limits do depend somewhat on dust temperature and spectral index. Based on the *Herschel* measurements, Lee et al. (2012) find that the average dust temperature is ~30 K under $\beta_{\rm d} = 1.5$ for relatively high redshift ($z \sim 4$) LBGs with a luminosity of $L \gtrsim 2\,L^*$ comparable to Himiko. In the local universe, the median dust temperatures are 33 K, 30 K, and 36 K, for E/S0, Sb-Sbc, and infrared bright galaxies, respectively (Sauvage & Thuan 1994; Young et al. 1989). Recent numerical simulations have claimed that LAEs may have a relatively high dust temperature, due to the proximity of dust to star-forming regions. However, even in this case, the maximum temperature reaches only $T_d \simeq 40$ K (Yajima et al. 2012b). On the other hand, Himiko's dust must be heated to some lower limit by the cosmic microwave background (CMB), whose blackbody temperature scales as $T_{\rm CMB}^{z=0}(1+z)$, where $T_{\rm CMB}^{z=0}$ is the temperature of the present-day CMB, $T_{\rm CMB}^{z=0} = 2.73$ K. Assuming local thermal equilibrium between the ISM of Himiko and the CMB at $z = 6.595$ (da Cunha et al. 2013) yields a lower limit of $T_d = 21$ K. Thus, it is appropriate to consider a range of $T_d \simeq 20$–40 K with $\beta_{\rm d} \simeq 1.5$. Because the larger assumed dust temperature $T_d = 40$ K with $\beta_{\rm d} = 1.5$ provides a weaker upper limit, we adopt a conservative 3σ upper limit of $L_{\rm FIR} < 8.0 \times 10^{10}\ L_\odot$ (8–1000 μm). Tables 1 and 3 present the 3σ luminosity upper limit.

3.2. ISM Metallicity from [C II] Emission

We now turn to estimating the metallicity of the ISM of Himiko using [C II] emission as a valuable tracer in star-forming regions. Despite our significant integration, no line is seen. Figure 6 (and Table 3) presents the upper limit to the [C II] luminosity in the context of the correlation with the SFR (de Looze et al. 2011). In the case of Himiko, the SFR was obtained by SED fitting of the rest-frame UV to optical data, including a correction for dust extinction (Section 3.3). Himiko clearly departs significantly from the scaling relation; the deficit amounts to a factor of $\simeq$ times 30. Given the SFRs of de Looze et al. (2011) for local galaxies are derived in a similar manner to that for Himiko, including contributions from dust-free and dusty starbursts with *Galaxy Evolution Explorer*'s UV and *Spitzer*'s infrared fluxes, respectively, it is difficult to believe that this deficiency is due to some form of bias arising from comparing different populations.

Graciá-Carpio et al. (2011) and Diaz-Santos et al. (2013) present $L_{\rm [C\,II]}/L_{\rm FIR}$ ratios for local starbursts that depend on $L_{\rm FIR}$ and the FIR and mid-IR surface brightnesses. As a result, Diaz-Santos et al. (2013) argue that $L_{\rm [C\,II]}$ may not represent a particularly reliable indicator of SFR. However, FIR and mid-IR luminosities only trace dusty starbursts and typically exclude dust-free measures such as the UV luminosity. Because galaxies with fainter FIR/mid-IR luminosities have a larger ratio of $L_{\rm [C\,II]}/L_{\rm FIR}$ in the datasets probed by Graciá-Carpio et al. (2011) and Diaz-Santos et al. (2013), more dust-free star-formation is expected in such systems. In this sense, the analysis of de Looze et al. (2011) is perhaps more relevant as a prediction of what to expect for Himiko. Nonetheless, given the importance of using

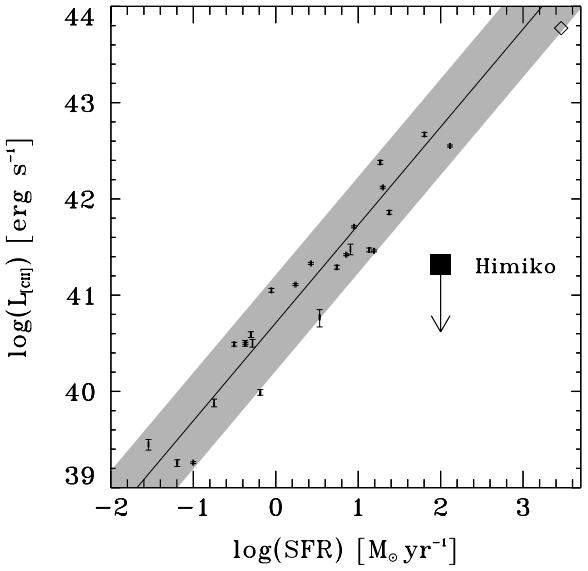

Figure 6. [C II] luminosity as a function of SFR. The filled square indicates the 3σ upper limit luminosity of Himiko and the open diamond presents estimates of HFLS3 (Riechers et al. 2013). The solid line is the local scaling relation determined with the data shown with bars (de Looze et al. 2011). Note that the bars are obtained by re-calculating the SFR values using the data of de Looze et al. (2011), following the formula shown in de Looze et al. (2011). The shaded region indicates the observed scatter.

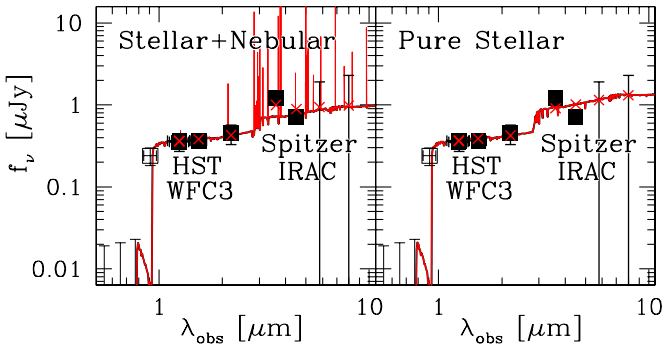

Figure 7. Optical to near-infrared SED of Himiko newly obtained by our deep *HST* and *Spitzer* observations, together with photometry from ground-based observations. The red lines represent the best-fit SEDs of stellar synthesis models with (left) and without (right) nebular lines (see Ono et al. 2010 for detailed model descriptions). The filled squares denote *HST* and *Spitzer*/SEDS fluxes of Himiko defined by the total magnitudes. The open squares show z'-band fluxes that are not used for the SED fitting, due to the Lyα line contamination. The large error bars at $\leqslant 0.8\,\mu$m and $>5\,\mu$m are those obtained by Subaru and *Spitzer*/SpUDS observations given by Ouchi et al. (2009b). The red crosses represent the broadband fluxes expected from the best-fit SED models. For various assumptions the fits indicate that Himiko has a SFR of 100 $M_\odot$ yr^{-1}, stellar mass of 2–3 $\times$ 10^{10} $M_\odot$, and a selective extinction of $E(B-V) = 0.15$ (see the text for details).

$L_{[\mathrm{C\,II}]}$ as a possible tracer and the discussion that follows below, independent studies of $L_{[\mathrm{C\,II}]}$ as a function of UV luminosity and L_{FIR} would be desirable. Figure 6 also shows that HFLS3 at $z = 6.3$ (Riechers et al. 2013) follows the local scaling relation. However, it should be noted that the SFR of HFLS3 is derived from the FIR luminosity, and thus any contribution from dust-free star-formation would be missing. In this sense, the SFR may be a lower limit, in which case HFLS3 may also depart somewhat from the local relation.

The absence of [C II] emission in Himiko is perhaps the most surprising result from our ALMA campaign. The emission line is often assumed to be the most robust far-IR tracer of star formation in high redshift galaxies, such that it may replace optical lines such as Lyα in securing spectroscopic redshifts in the reionization era. Our failure to detect this line in one of the most spectacular $z \simeq 7$ galaxies has significant implications, which we discuss in Section 4.

3.3. Improved Physical Properties from the Near-infrared SED

Although we derived some constraints on the integrated properties of Himiko in our earlier work (Ouchi et al. 2009b), we did not obtain an $E(B-V)$ estimate and only the lower limit of SFR with $E(B-V) \geqslant 0$ was obtained, due to the large uncertainties of photometric measurements. We now refine these estimates based on our significantly deeper *HST* and *Spitzer* data. Our near-IR SED is taken using total magnitudes from the *HST* images (Section 2.2), the *Spitzer*/IRAC SEDS images (Section 2.3), and *JHK* DR8 data from the UKIDSS/UDS survey. We tabulate these total magnitudes in Table 3 including ground-based optical data previously given in Ouchi et al. (2009b).

We present the SED of Himiko in Figure 7 and undertake the χ^2 fitting of a range of stellar synthesis models in the same manner as Ono et al. (2010b), using the stellar synthesis models of Bruzual & Charlot (2003) with the dust attenuation formulation given by Calzetti et al. (2000). We adopt a Salpeter initial mass function (IMF; Salpeter 1955) with lower and upper mass cutoffs of 0.1 and 100 $M_\odot$, respectively. Applying models of constant and exponentially decaying star-formation histories with metallicities ranging from $Z = 0.02$–$1.0\ Z_\odot$, we search for the best-fit model in a parameter space of $E(B-V) = 0$–1 and age = 1–810 Myr (where the latter upper limit corresponds to the cosmic age at $z = 6.595$). Nebular continuum and line emission, estimated from the ionizing photons from young stars, are optionally included following the metallicity-dependent prescriptions presented in Schaerer & de Barros (2009) and Ono et al. (2010b).

For a constant SFR history with no nebular emission and a fixed metallicity of $Z = 0.2\ Z_\odot$, we find that our best-fit model has a stellar mass of $M_* = 3.0^{+0.4}_{-0.6} \times 10^{10}\ M_\odot$, a stellar age of $3.6^{+0.4}_{-0.8} \times 10^8$ yr, a SFR of $98^{+2}_{-2}\ M_\odot$ yr^{-1}, and an extinction of $E(B-V) = 0.15$ with a reduced χ^2 of 3.1. This is a significant improvement over our much weaker earlier constraints which did not have the benefit of the *HST*/WFC3 or *Spitzer*/SEDS data(Ouchi et al. 2009b). The new infrared data play a critical role in determining the Balmer break, thereby resolving the degeneracy between extinction and age. On the other hand, the fit itself is not very satisfactory. The reduced χ^2 is large and there is a significant discrepancy at 3.6 μm. Since the 3.6 μm and 4.5 μm bands sample the strong nebular lines of Hβ+[O III] and Hα, respectively, at $z = 6.595$, this encourages us to include nebular emission in our fitting procedure. In fact, in Figure 4, we note that the IRAC 4.5 μm emission shows a positional offset with respect to that at 3.6 μm, suggesting the possibility of contamination by nebular emission.

Adding nebular emission to the stellar SED models given above, the best fit has a more satisfactory reduced χ^2 of 1.6, and we derive a reduced stellar mass of $M_* = 1.5^{+0.2}_{-0.2} \times 10^{10}\ M_\odot$ and a younger stellar age of $1.8^{+0.2}_{-0.2} \times 10^8$ yr, but similar values for the SFR of $100^{+2}_{-2}\ M_\odot$ yr^{-1} and extinction of $E(B-V) = 0.15$. Table 4 summarizes the results of our SED fitting with the pure stellar and stellar+nebular models. In the stellar+nebular models, we assume that all ionizing photons lead to nebular emission lines corresponding to an escape fraction $f_{\mathrm{esc}} = 0$. If we allow f_{esc} to be a free parameter, then following

Table 4
Stellar Population of Himiko

Model	M_* ($M_\odot$)	$E(B-V)_*$ (mag)	Age (Myr)	SFR ($M_\odot$ yr^{-1})	sSFR (yr^{-1})	χ^2/dof
(1)	(2)	(3)	(4)	(5)	(6)	(7)
Stellar+nebular	$1.5^{+0.2}_{-0.2} \times 10^{10}$	0.15[a]	182^{+22}_{-20}	100 ± 2	$6.7 \pm 0.9 \times 10^{-9}$	1.55
Pure stellar	$3.0^{+0.4}_{-0.6} \times 10^{10}$	0.15[a]	363^{+44}_{-75}	98 ± 2	$3.3 \pm 0.5 \times 10^{-9}$	3.13

Notes. Columns: (1) models with or without nebular emission. (2) Stellar mass. (3) Color excess of dust extinction for stellar continua. (4) Stellar age. (5) Star-formation rate. (6) Specific star-formation rate. (7) Reduced χ^2. The degree of freedom (dof) is six.
[a] The uncertainty of color excess is smaller than our model-parameter grid of $\Delta E(B-V) = 0.01$.

Ono et al. (2012b) we find no change from the model above (i.e., $f_{\rm esc} = 0$) and formally establish that $f_{\rm esc} < 0.2$.

Labbé et al. (2010) and Finkelstein et al. (2010) have suggested from their pure stellar models that *HST* $z = 7$–8 dropout galaxies have modest stellar masses (10^8–10^9 $M_\odot$) and are quite young (30–300 Myr), in contrast with Himiko's stellar mass ($M_* \simeq 3.0 \times 10^{10}$ $M_\odot$) and age (360 Myr) estimated with our pure stellar models. Of course, Himiko is more massive and energetic than typical LBGs seen in the small area of the Hubble Ultra Deep Field. Its most notable feature is its high SFR of $\simeq$100 $M_\odot$ yr^{-1}, which is more than an order of magnitude larger than those of the *HST* LBGs at similar redshifts ($\simeq$1–10 $M_\odot$ yr^{-1}; Labbé et al. 2010). Himiko's selective extinction, $E(B-V) = 0.15$, is also larger than that of *HST* dropouts, more than half of which are consistent with no extinction (Finkelstein et al. 2010). On the other hand, the stellar mass of Himiko is only about 1/10th that of many sub-millimeter galaxies (SMGs) at $z \sim 3$ (Chapman et al. 2005). We estimate a specific star-formation rate (sSFR), defined by a ratio of SFR to stellar mass, to be sSFR $= 3.3 \pm 0.5 \times 10^{-9}$ and sSFR $= 6.7 \pm 0.9 \times 10^{-9}$ yr^{-1}, for the pure stellar and stellar+nebular cases, respectively. Even though the stellar masses are very different, Himiko, SMGs, and LBGs at $z \sim 3$ share comparable sSFRs $\sim 10^{-9}$–10^{-8} yr^{-1} (see Figure 12 of Ono et al. 2010a).

3.4. UV Spectral Slopes on the Spatially Resolved Images

The new *HST* data give us the first reliable measurement of the UV continuum slope for each of the morphological components identified in Figure 4. The UV spectral slope provides a valuable indicator of the combination of dust extinction, metallicity, the upper IMF, and stellar age. We estimated the UV slope, β, from the J_{125} and H_{160} photometry, which samples the continua at the rest-frame wavelengths of $\sim$1600 and $\sim$2100 Å, neither of which is contaminated by either Lyα emission or the Lyα-continuum break.

We calculate β via

$$\beta = -\frac{J_{125} - H_{160}}{2.5 \log\left(\lambda_c^1/\lambda_c^2\right)} - 2, \quad (1)$$

where λ_c^1 and λ_c^2 are the central wavelengths of the J_{125} and H_{160} filters, respectively. The estimates for each component are summarized in Table 2. We obtain $\beta = -2.00 \pm 0.57$ for the entire system of Himiko, which is comparable to the average UV slope of $\simeq L^*$ LBGs, $\beta = -2.09 \pm 0.22$ (Bouwens et al. 2012, see also Dunlop et al. 2013). Figure 8 shows the UV-to-FIR luminosity ratio, $\log(L_{\rm FIR}/L_{1600})$, and the UV-continuum slope, β, for the entire system of Himiko, and compares these

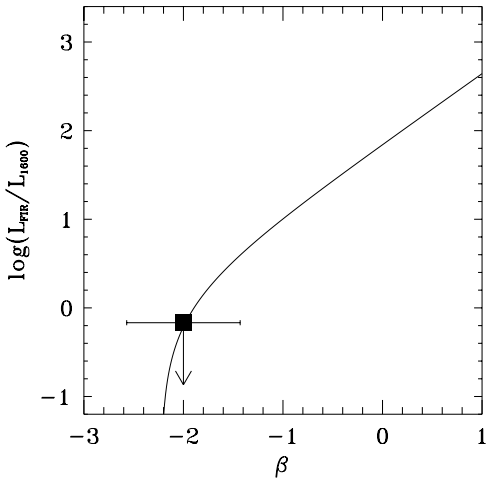

Figure 8. UV to FIR luminosity ratio, $\log(L_{\rm FIR}/L_{1600})$, as a function of the UV-continuum slope, β. The filled square presents the upper limit of $\log(L_{\rm FIR}/L_{1600})$ and the measurement of β for the total luminosities of Himiko. The solid line denotes the relation for local starbursts given by Meurer et al. (1999).

estimates with the relation of local starbursts (Meurer et al. 1999). Figure 8 indicates that Himiko has $\log(L_{\rm FIR}/L_{1600})$-$\beta$ values comparable with or smaller than those of local dust-poor starbursts. Since the Small Magellanic Cloud (SMC) extinction has a smaller $\log(L_{\rm FIR}/L_{1600})$ value at a given β (see Figure 10 of Reddy et al. 2010) due to SMC's steeper extinction curve in $A_\lambda/A_{\rm V}$-1/λ than that for local starbursts, it may be more appropriate for Himiko. Our result also suggests that Himiko is not associated with additional FIR sources that are invisible in the rest-frame UV. These implications are consistent with the conclusions of the UV-FIR luminosity ratio discussed in Figure 5.

More interestingly, the UV slopes of the individual substructures provide valuable information on the nature of Himiko. Clumps B and C have $\beta = -2.04 \pm 0.47$ and $\beta = -2.22 \pm 0.28$, respectively, which are comparable to the average UV slope of $\simeq L^*$ LBGs. However, Clump A presents a very blue UV slope, $\beta = -2.84 \pm 0.32$. Because this component is detected at the $\sim 20\sigma$ level in both J_{125} and H_{160}, the UV slope is quite reliable. Bouwens et al. (2012) claim that selection and photometric biases lead to an error of only $\Delta\beta \simeq +0.1$ for the brightest of their sources with $\sim 20\sigma$ photometry (see also Dunlop et al. 2013). Even including such a possible bias, Clump A remains significantly bluer than the average $\simeq L^*$ LBGs at the $\simeq 2\sigma$ level.

As presented in Section 2.2, Clump A also shows Lyα emission. Together with the blue UV slope, this suggests a

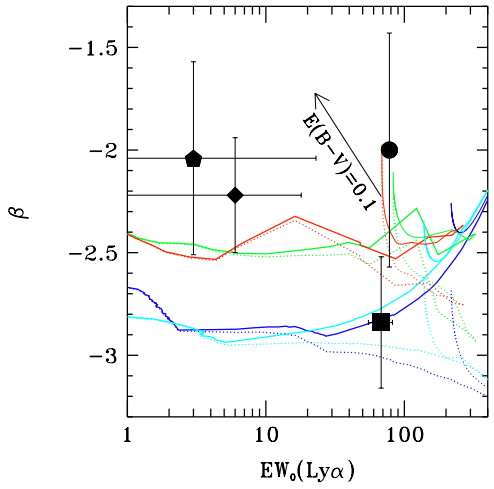

Figure 9. UV-continuum slope, β, as a function of rest-frame Lyα equivalent width. The filled circle, square, pentagon, and diamond denote measures for the entire system, and Clumps A, B, and C, respectively. The blue, cyan, green, and red solid lines represent predictions based on instantaneous starburst models of PopIII, $Z = 10^{-5}$ $Z_\odot$, 0.01 $Z_\odot$, and 0.2 $Z_\odot$ with nebular and stellar continua (Raiter et al. 2010). The thin lines are the same, but for constant star-formation models. The associated dotted lines show the effect of ignoring nebular emission. The arrow indicates the effect of applying an extinction with $E(B-V)_s = 0.1$ (see the text for details).

very young and/or metal poor component. However, the Lyα equivalent width is only $EW_0 = 68^{+14}_{-13}$ Å. To understand the significance of this, in Figure 9, we compare β and EW_0 for the entire Himiko system and the various clumps with the stellar and nebular models of Raiter et al. (2010), where a Salpeter IMF is assumed. In Figure 9, the arrow size in β for the stellar extinction of $E(B-V)_s = 0.1$ is calculated using a combination of the empirical relation, $A_{1600} = 4.43 + 1.99\beta$ (Meurer et al. 1999), and Calzetti extinction, $A_{1600} = k_{1600}E(B-V)_s$, where k_{1600} is 10 (Ouchi et al. 2004). Similarly, the arrow size in EW_0 for $E(B-V)_s = 0.1$ is estimated from the relation given in Ono et al. (2010a) under the assumption of a f_ν flat continuum and the standard SFR relations of UV and Lyα luminosities in the case of B recombination. Figure 9 shows that the data points of Himiko fall on the tracks of star-formation photoionization models (Raiter et al. 2010) within the measurement errors and the dust-extinction correction uncertainties, and indicates that the Lyα emission of Himiko can be explained by photoionization by massive stars.

4. DISCUSSION

We now bring together our key results, both from the earlier Subaru program (Ouchi et al. 2009b) and the present *HST* and ALMA campaigns, in order to understand the significance of our upper limits on the [C II] and dust emission, and thereby the nature of Himiko.

4.1. The Low Dust and Metal Content of Himiko

We have shown (Figure 5) that Himiko's sub-millimeter emission is comparable with or weaker than that of local dwarf irregulars with far lower SFRs, indicating intensive star-formation in a dust-poor gaseous environment. In fact, assuming the local starburst SFR–L(FIR) relation of Kennicutt (1998) with Himiko's FIR upper limit luminosity of $<8 \times 10^{10}$ $L_\odot$, we obtain SFR(FIR) < 14 $M_\odot$ yr^{-1}, which is far smaller than not only our best optical-NIR estimate SFR of $\simeq 100$ $M_\odot$ yr^{-1}, but also the UV-luminosity SFR of SFR(UV) $= 30 \pm 2$ $M_\odot$ yr^{-1} with no dust extinction correction. This is also true under the assumption of the SFR–L(FIR) relation (Buat & Xu 1996) which is valid for local dust poor disk systems of Sb and later galaxies, which provides SFR(FIR) < 25 $M_\odot$ yr^{-1}. In this way, Himiko does not follow the SFR–L(FIR) relation of typical local galaxies, indicating a dust-poor gaseous environment. This seems similar to observations that find extended Lyα emission in dust poor low-z galaxies (Hayes et al. 2013) and a high-z QSO (Willott et al. 2013). Based on numerical simulations, Dayal et al. (2010) find that $z \sim 6$–7 LAEs are dust poor with a dust-to-gas mass ratio smaller than the Milky Way by a factor of 20. Dayal et al. (2010) predict a 1.4 mm continuum flux of $\simeq 50$ μJy for sources with L(Lyα) $= 2$–3×10^{43} erg s^{-1} at $z = 6.6$, a result comparable to our ALMA observations. Deeper ALMA observations could further test the model of Dayal et al. (2010) and place important constraints on the dust-to-gas mass ratio.

Similarly, our strong upper limit on the [C II] 158 μm line (Figure 6) places it significantly below the scaling relation of $L_{[C\,II]}$ and SFR that is obeyed by lower redshift galaxies. This discovery indicates the following four possibilities: Himiko has (1) a hard ionizing spectrum from an AGN, (2) a very high density of photo-dissociation regions (PDRs), (3) a low metallicity, and (4) a large column density of dust. In case (1), a hard ionizing spectrum from an AGN can produce little [C II] luminosity relative to FIR luminosity, due to the intense ionization field (Stacey et al. 2010). As we discuss in (2) of Section 4.2, there are no AGN signatures; there are no detections of X-ray and high-ionization lines, as well as extended sources plus non-AGN-like Lyα profile+surface brightness. We can rule out possibility (1). In case (2), a very high density of PDRs provides more rapid collisional de-excitations for the forbidden line of [C II], and quenches a [C II] emission line. In case (3), the PDRs in Himiko are composed of metal poor gas that may be quite typical of normal galaxies observed at early epochs. De Looze (2012) has argued that offsets from the [C II]–SFR relation can be explained in terms of metal abundance and this would imply a gas-phase metallicity of $\lesssim 0.03$ $Z_\odot$. Indeed, for our young mean stellar age of 160–410 Myr, standard ionization-photon bounded HII regions with a local chemical abundance would yield [C II] emission somewhat above the local scaling relation, due to the expected large PDRs. Moreover, the recent numerical simulations predict that a [C II] flux drops as metallicity decreases (Vallini et al. 2013). Vallini et al. (2013) claim that Himiko's gas-phase metallicity is sub-solar on the basis of the comparison of their models with the previous IRAM [C II] upper limit. Comparing these numerical models with our strong ALMA upper limit of [C II] would place further constraints on the metallicity of Himiko. In case (4), the depth of C^+ zones in PDRs is determined by dust extinction. Since the C^+ zones extend over the dust extinction up to $A_v \leqslant 4$ (Malhotra et al. 2001), heavy dust extinction in the ISM does not allow the creation of a large C^+ zones emitting [C II]. However, from the no detection of a 1.2 mm dust continuum discussed above, the heavy dust extinction narrowing the PDRs is unlikely. As dust extinction and gas phase metallicity generally correlate closely (Storchi-Bergmann et al. 1994; see also Finlator et al. 2006), the weak dust emission also suggests a very low metallicity gas. Thus, case (3) is probably true, which contributes the weak [C II] emission. Case (2) could also help to weaken the [C II] emission. To summarize, faint [C II] and weak dust emission can be explained in a self-consistent manner with a very low metallicity gas and little dust in a near-primordial system.

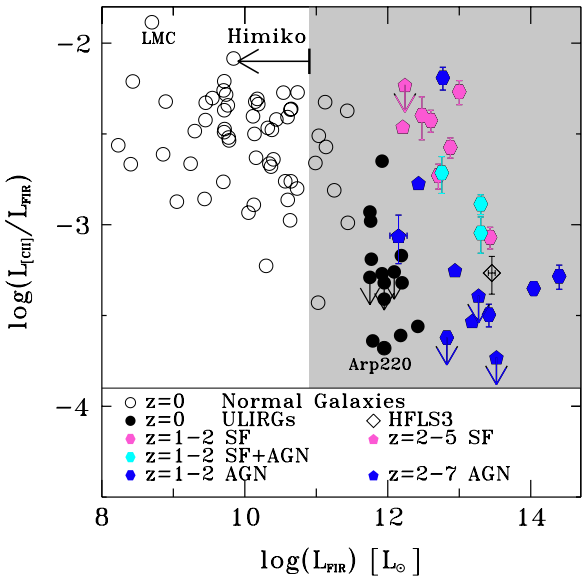

Figure 10. Ratio of [C II] luminosity to FIR luminosity as a function of FIR luminosity. The thick bar with the arrow presents the FIR upper limit for Himiko at the arbitrary position in the vertical axis, and the gray shaded region denotes the excluded range. The ratios for star-forming (SF) and AGN-dominated galaxies at $z = 1$–2 are shown with magenta and blue pentagons, respectively, while those of the intermediate SF+AGN population at $z = 1$–2 are represented with cyan hexagons (Stacey et al. 2010). Similarly, SF and AGN dominated galaxies at $z > 2$ are indicated by the magenta pentagons and blue hexagons, respectively (Marsden et al. 2005; Maiolino et al. 2005, 2009; Iono et al. 2006; Pety et al. 2004; Ivison et al. 2010; Venemans et al. 2012). The black open diamond represents HFLS3 at $z = 6.3$ (Riechers et al. 2013). The black open and filled circles denote local normal galaxies (Malhotra et al. 2001) and ULIRGs (Maiolino et al. 2005 and references therein), respectively, together with well-known local galaxies of the LMC, M82, and Arp220.

It is informative to compare the above conclusion with the only other well-studied galaxy at this redshift, HFLS3 at $z = 6.34$ (Riechers et al. 2013), recognizing that both this galaxy and Himiko were selected based on their extreme properties. Figure 10 presents the ratio of [C II] to the FIR luminosity as a function of FIR luminosity. Although Himiko is significantly offset from the trend shown by AGN and local starbursts, this is not the case for HFLS3. Although Riechers et al. (2013) claim that HFLS3 is free from AGN activity based on the level of excitation for CO and H_2O, its small [C II] to $L_{\rm FIR}$ ratio of $L_{\rm [C\,II]}/L_{\rm FIR} = 5 \times 10^{-4}$ suggests otherwise (Stacey et al. 2010; Sargsyan et al. 2012). On the other hand, the recent study of Diaz-Santos et al. (2013) finds that a luminous infrared galaxy (LIRG) with compact star-forming regions show a smaller $L_{\rm [C\,II]}/L_{\rm FIR}$ value, and that a $L_{\rm [C\,II]}/L_{\rm FIR}$ value of pure star-forming LIRG drops by an order of magnitude, from 10^{-2} to 10^{-3}. Thus, there is the other possibility that HFLS3 could be a pure star-forming source that is more compact than those of local pure star-forming LIRGs.

4.2. Nature of Himiko

In considering the origin of Himiko's extreme SFR and extensive Lyα halo, it is convenient to return to the various explanations originally proposed by Ouchi et al. (2009b) on the basis of the Subaru, UKIDSS, and shallow *Spitzer* data available at the time, taking into account the progress achieved with our new deep ALMA, *HST*, and *Spitzer* data.

1. *A Gravitationally Lensed Source.* Ouchi et al. (2009b) discounted this possibility on the basis of the resolved kinematics of the extended Lyα halo. In Section 2.2, we have strengthened the objections to this hypothesis since our *HST* data reveal three L^* sources whose morphological asymmetries are not consistent with gravitational lensing. Moreover, we can find no potential foreground lens in the vicinity of Himiko (Ouchi et al. 2009b). Such a lens would have to be one of the three clumps revealed in the *HST* images, each of which has a 0.9 μm-continuum break and a blue UV continuum consistent with being physically associated at $z \simeq 6.6$. Our deep IRAC data also show no potential lensing sources near Himiko, suggesting that there are no lensing objects with very red color, such as dusty starbursts at intermediate redshifts, which are invisible in the optical and NIR bands. Thus, we conclude that Himiko is not a gravitational lensed system.
2. *Halo gas ionized by a hidden AGN.* Our *HST* images do not reveal any obvious point source that could represent an active nucleus (Figure 4). Moreover, as noted by Ouchi et al. (2009b), Himiko is undetected at X-ray wavelengths of 0.5–2 keV down to 6×10^{-16} erg s^{-1} cm^{-2}, and the Keck optical spectrum does not reveal any high ionization features such as Nv. Finally, radiative transfer simulations by Baek & Ferrara (2013) show that the Lyα line profile and surface brightness of Himiko are inconsistent with heating from either a Compton-thick or Compton-thin AGN. Thus, we conclude the Lyα halo is unlikely to be heated by an AGN.
3. *Clouds of* H II *regions in a single virialized galaxy.* Ouchi et al. (2009b) discussed the possibility that Himiko could be a single virialized system. Since the new *HST* data reveals three distinct UV luminous clumps, each comparable to the characteristic luminosity L^*, we consider that Himiko is unlikely to be a single virialized system Although there are many reports of disk galaxies with prominent clumps at $z \sim 2$–3 (e.g., Genzel et al. 2011), the absence of a stellar disk (Figure 4) distinguishes Himiko from a single galaxy with clumpy structures such as those found at lower redshifts.
4. *Cold gas accretion onto a massive dark halo producing a central starburst.* Some theoretical studies have suggested that cold gas can efficiently penetrate into the central regions of a dark halo if that halo is more massive than the shock-heating scale of $\sim$4–7 $\times 10^{11}\,M_\odot$ at $z > 4$ (Dekel et al. 2009; Ocvirk et al. 2008). Given Himiko's stellar mass (1.5–3 $\times 10^{10}\,M_\odot$, Section 3.3) and little or no evolution in the ratio of stellar mass, M_*, to halo mass inferred for $0 < z < 1$ ($M_*/M_{\rm DH} \lesssim 0.05$, Leauthaud et al. (2012)), we expect a halo mass of $M_{\rm DH} \gtrsim$ 3–6 $\times 10^{11}\,M_\odot$. Abundance matching considerations support this estimate. Ouchi et al. (2009b) calculated that there should be at least one halo of mass $10^{12}\,M_\odot$ in the survey volume of 8×10^5 comoving Mpc^3 where Himiko was found (see also Behroozi et al. 2012).

   Although Himiko's halo mass does likely lie in the range where cold accretion could be possible, we note that some recent simulations have cast doubt on the efficiency of this mode of assembly (Nelson et al. 2013; Vogelsberger et al. 2013).
5. *Outflowing gas excited by shocks or UV radiation from starbursts and/or mergers.* The extensive Lyα nebula may be powered by star formation itself, but the gas could also be shock heated by strong outflows driven by multiple supernova explosions in an intensive starburst (Mori et al.

2004). Figure 9 shows the relation between the UV slope β, which characterizes the stellar population and the Lyα equivalent width EW_0. This shows that the photoionization models of Raiter et al. (2010) whereby Lyα photons are scattered by the ISM and circum-galactic medium can explain the properties of Himiko, notwithstanding the uncertainties in β. The success of this model depends, of course, on the escape fraction of ionizing photons which should be moderately low (<50%) so that scattering is effective. However, the conclusion is robust even if we adopt a moderate dust extinction of $E(B-V)_s = 0.15$ (Section 3.3).

Thus, within the uncertainties, the amount of star formation observed is sufficient to power the extended Lyα nebula; outflow and shocks are not required. This simple photoionization scenario is consistent with the negligible hidden star-formation suggested by the weak dust and carbon emission from our ALMA observations. As discussed in Ouchi et al. (2009b), the FWHM of the Lyα line is only $v_{\rm FWHM} = 251 \pm 21$ km s^{-1}, further indicating that powerful outflows are not present.

6. *Merging bright galaxies.* Although this is not a separate hypothesis from (5) above, we can ask what triggers the intense star formation that likely powers the extended nebula. In Figure 4, we have identified three L^* clumps that are highly suggestive of a rare triple merger. As Ouchi et al. (2009b) reported, Himiko presents a small velocity offset of Lyα emission across the nebula ($\Delta v = 60$ km s^{-1}) with a narrow line width ($v_{\rm FWHM} = 251$ km s^{-1}; see Figure 7 of Ouchi et al. 2009a for the Lyα line velocities that are measured on the slit position shown with the red box in Figure 1 of Ouchi et al. 2009a). Thus, the merger would have to be largely confined to the direction perpendicular to the line of sight.

Although a triple major merger is a rare event, our data suggest that this explanation is the most plausible. Recent numerical simulations predict that some extended Lyα sources originate in mergers (Yajima et al. 2012a). One interesting feature of Himiko is that the brightest portion of the Lyα nebula does not coincide with the geometric center of the three clumps, but is located between the blue Lyα clump A and clump B. Given the discussion in (5) above, this indicates that Lyα photons are mainly produced by Clump A, a very young and metal poor component.

5. SUMMARY

We have taken deep ALMA and *HST*/WFC3-IR data and supplementary *Spitzer* SEDS photometry for the remarkably luminous star-forming galaxy, Himiko, at $z = 6.595$, which has an extended Lyα nebula at $z \sim 7$. Following the original discovery (Ouchi et al. 2009b),these new data provide valuable insight into its physical properties, and thereby offer a unique perspective on how the earliest massive galaxies formed. We summarize our conclusions as follows.

1. The 1.2 mm dust continuum flux from this star-forming galaxy is very weak, <52 μJy, and comparable with or weaker than that observed for local dwarf irregulars with much lower SFRs.
2. We find a surprisingly stringent upper limit to the flux of the [C II] 158 μm line, $L_{\rm [C\,II]} < 5.4 \times 10^7\ L_\odot$, placing it a factor $\simeq$30 below expectations based on the scaling relation established between $L_{\rm [C\,II]}$ and SFR for lower redshift galaxies. This indicates a very metal poor system and may imply that the [C II] line will be a poor diagnostic of early $z > 7$ galaxies.
3. Our deeper *HST*+*Spitzer* photometry allows us to considerably refine the stellar population properties of Himiko. Using models with and without nebular lines, we infer a stellar mass of 1.5–3 $\times 10^{10}\ M_\odot$ and a SFR of $\simeq 100 \pm 2\ M_\odot$ yr^{-1}, comparable with the properties of luminous LBGs at $z \sim 3$.
4. Our *HST* image has revealed three L^* galaxy clumps which, together with our earlier kinematic constraints, suggest a rare triple merger. One clump reveals intense Lyα emission and an extremely blue color continuum of $\beta = -2.84 \pm 0.32$, which is suggestive of metal-poor star-formation and an age of less than 200 Myr.
5. From these properties, we conclude that we are witnessing intense star formation induced by this triple merger and that the associated photoionizing radiation is sufficient to power the extensive Lyα nebula.

Although it is a rare object, Himiko has offered us the first coherent view of how the most massive galaxies started forming at a time close to the end of cosmic reionization at $z \sim 7$.

We are grateful to Pratika Dayal, Andrea Ferrara, Rob Kennicutt, Kyoungsoo Lee, Masao Mori, Dominik Riechers, Dimitra Rigopoulou, Daniel Schaerer, Masayuki Umemura, Fabian Walter, and Chris Willott for their useful comments and discussions. We thank the ALMA observatory and *HST* support staff for their invaluable help that made these pioneering observations possible. The *HST* reduction was supported by a NASA STScI grant GO 12265. This work was supported by World Premier International Research Center Initiative (WPI Initiative), MEXT, Japan, and KAKENHI (23244025) Grant-in-Aid for Scientific Research (A) through Japan Society for the Promotion of Science (JSPS). This paper makes use of the following ALMA data: ADS/JAO.ALMA#2011.0.00115.S. ALMA is a partnership of ESO (representing its member states), NSF (USA), and NINS (Japan), together with NRC (Canada), NSC, and ASIAA (Taiwan), in cooperation with the Republic of Chile. The Joint ALMA Observatory is operated by ESO, AUI/NRAO, and NAOJ. This work is based on observations made with the NASA/ESA *Hubble Space Telescope*, obtained at the Space Telescope Science Institute, which is operated by the Association of Universities for Research in Astronomy, Inc., under NASA contract NAS 5-26555. These observations are associated with program #12265. Support for program #12265 was provided by NASA through a grant from the Space Telescope Science Institute, which is operated by the Association of Universities for Research in Astronomy, Inc., under NASA contract NAS 5-26555. This work is based in part on observations made with the *Spitzer Space Telescope*, which is operated by the Jet Propulsion Laboratory, California Institute of Technology under a contract with NASA. Support for this work was provided by NASA through an award issued by JPL/Caltech.

Facilities: ALMA (Band6) *HST* (WFC3-IR) *Spitzer* (IRAC)

REFERENCES

Ashby, M. L. N., Willner, S. P., Fazio, G. G., et al. 2013, ApJ, 769, 80
Baek, S., & Ferrara, A. 2013, MNRAS, 432, 6
Behroozi, P. S., Wechsler, R. H., & Conroy, C. 2013, ApJ, 770, 57
Bouwens, R. J., Illingworth, G. D., Oesch, P. A., et al. 2010a, ApJL, 709, L133
Bouwens, R. J., Illingworth, G. D., Oesch, P. A., et al. 2010b, ApJL, 708, L69
Bouwens, R. J., Illingworth, G. D., Oesch, P. A., et al. 2011, ApJ, 737, 90
Bouwens, R. J., Illingworth, G. D., Oesch, P. A., et al. 2012, ApJ, 754, 83

Bruzual, G., & Charlot, S. 2003, MNRAS, 344, 1000
Buat, V., & Xu, C. 1996, A&A, 306, 61
Calzetti, D., Armus, L., Bohlin, R. C., et al. 2000, ApJ, 533, 682
Capak, P. L., Riechers, D., Scoville, N. Z., et al. 2011, Natur, 470, 233
Castellano, M., Fontana, A., Boutsia, K., et al. 2010, A&A, 511, A20
Chapman, S. C., Blain, A. W., Smail, I., & Ivison, R. J. 2005, ApJ, 622, 772
Coppin, K. E. K., Chapman, S. C., Smail, I., et al. 2010, MNRAS, 407, L103
da Cunha, E., Groves, B., Walter, F., et al. 2013, ApJ, 766, 13
Dale, D. A., Gil de Paz, A., Gordon, K. D., et al. 2007, ApJ, 655, 863
Dayal, P., Maselli, A., & Ferrara, A. 2011, MNRAS, 410, 830
Dekel, A., Birnboim, Y., Engel, G., et al. 2009, Natur, 457, 451
De Looze, I. 2012, Ph.D. thesis, Universiteit Gent.
de Looze, I., Baes, M., Bendo, G. J., Cortese, L., & Fritz, J. 2011, MNRAS, 416, 2712
Diaz-Santos, T., Armus, L., Charmandaris, V., et al. 2013, ApJ, 774, 68
Dunlop, J. S., McLure, R. J., Robertson, B. E., et al. 2012, MNRAS, 420, 901
Dunlop, J. S., Rogers, A. B., McLure, R. J., et al. 2013, MNRAS, 432, 3520
Eales, S. A., Wynn-Williams, C. G., & Duncan, W. D. 1989, ApJ, 339, 859
Ellis, R. S., McLure, R. J., Dunlop, J. S., et al. 2013, ApJL, 763, L7
Finkelstein, S. L., Papovich, C., Giavalisco, M., et al. 2010, ApJ, 719, 1250
Finlator, K., Davé, R., Papovich, C., & Hernquist, L. 2006, ApJ, 639, 672
Genzel, R., Newman, S., Jones, T., et al. 2011, ApJ, 733, 101
Graciá-Carpio, J., Sturm, E., Hailey-Dunsheath, S., et al. 2011, ApJL, 728, L7
Hayes, M., Östlin, G., Schaerer, D., et al. 2013, ApJL, 765, L27
Holland, W. S., Robson, E. I., Gear, W. K., et al. 1999, MNRAS, 303, 659
Iono, D., Yun, M. S., Elvis, M., et al. 2006, ApJL, 645, L97
Ivison, R. J., Swinbank, A. M., Swinyard, B., et al. 2010, A&A, 518, L35
Kanekar, N., Wagg, J., Ram Chary, R., & Carilli, C. 2013, ApJ, 771, 20
Kennicutt, R. C., Jr. 1998, ARA&A, 36, 189
Klaas, U., Haas, M., Heinrichsen, I., & Schulz, B. 1997, A&A, 325, L21
Labbé, I., González, V., Bouwens, R. J., et al. 2010, ApJL, 716, L103
Leauthaud, A., Tinker, J., Bundy, K., et al. 2012, ApJ, 744, 159
Lee, K.-S., Alberts, S., Atlee, D., et al. 2012, ApJL, 758, L31
Maiolino, R., Caselli, P., Nagao, T., et al. 2009, A&A, 500, L1
Maiolino, R., Cox, P., Caselli, P., et al. 2005, A&A, 440, L51
Malhotra, S., Kaufman, M. J., Hollenbach, D., et al. 2001, ApJ, 561, 766
Marsden, G., Borys, C., Chapman, S. C., Halpern, M., & Scott, D. 2005, MNRAS, 359, 43
McLure, R. J., Dunlop, J. S., Bowler, R. A. A., et al. 2013, MNRAS, 432, 2696
McLure, R. J., Dunlop, J. S., Cirasuolo, M., et al. 2010, MNRAS, 403, 960
Meurer, G. R., Heckman, T. M., & Calzetti, D. 1999, ApJ, 521, 64
Mori, M., Umemura, M., & Ferrara, A. 2004, ApJL, 613, L97
Nelson, D., Vogelsberger, M., Genel, S., et al. 2013, MNRAS, 429, 3353
Ocvirk, P., Pichon, C., & Teyssier, R. 2008, MNRAS, 390, 1326
Oesch, P. A., Bouwens, R. J., Illingworth, G. D., et al. 2010, ApJL, 709, L16
Ono, Y., Ouchi, M., Curtis-Lake, E., et al. 2012a, arXiv:1212.3869
Ono, Y., Ouchi, M., Mobasher, B., et al. 2012b, ApJ, 744, 83
Ono, Y., Ouchi, M., Shimasaku, K., et al. 2010a, MNRAS, 402, 1580
Ono, Y., Ouchi, M., Shimasaku, K., et al. 2010b, ApJ, 724, 1524
Ouchi, M., Mobasher, B., Shimasaku, K., et al. 2009a, ApJ, 706, 1136
Ouchi, M., Ono, Y., Egami, E., et al. 2009b, ApJ, 696, 1164
Ouchi, M., Shimasaku, K., Furusawa, H., et al. 2010, ApJ, 723, 869
Ouchi, M., Shimasaku, K., Okamura, S., et al. 2004, ApJ, 611, 660
Ouchi, M., Yamada, T., Kawai, H., & Ohta, K. 1999, ApJL, 517, L19
Pety, J., Beelen, A., Cox, P., et al. 2004, A&A, 428, L21
Raiter, A., Schaerer, D., & Fosbury, R. A. E. 2010, A&A, 523, A64
Reddy, N. A., Erb, D. K., Pettini, M., Steidel, C. C., & Shapley, A. E. 2010, ApJ, 712, 1070
Reddy, N. A., & Steidel, C. C. 2009, ApJ, 692, 778
Riechers, D. A., Bradford, C. M., Clements, D. L., et al. 2013, Natur, 496, 329
Riechers, D. A., Capak, P. L., Carilli, C. L., et al. 2010, ApJL, 720, L131
Robertson, B. E., Furlanetto, S. R., Schneider, E., et al. 2013, ApJ, 768, 71
Salpeter, E. E. 1955, ApJ, 121, 161
Sargsyan, L., Lebouteiller, V., Weedman, D., et al. 2012, ApJ, 755, 171
Sauvage, M., & Thuan, T. X. 1994, ApJ, 429, 153
Schaerer, D., & de Barros, S. 2009, A&A, 502, 423
Schaerer, D., & de Barros, S. 2010, A&A, 515, A73
Schenker, M. A., Robertson, B. E., Ellis, R. S., et al. 2013, ApJ, 768, 196
Silva, L., Granato, G. L., Bressan, A., & Danese, L. 1998, ApJ, 509, 103
Stacey, G. J., Hailey-Dunsheath, S., Ferkinhoff, C., et al. 2010, ApJ, 724, 957
Storchi-Bergmann, T., Calzetti, D., & Kinney, A. L. 1994, ApJ, 429, 572
Vallini, L., Gallerani, S., Ferrara, A., & Baek, S. 2013, MNRAS, 433, 1567
Venemans, B. P., McMahon, R. G., Walter, F., et al. 2012, ApJL, 751, L25
Vieira, J. D., Marrone, D. P., Chapman, S. C., et al. 2013, Natur, 495, 344
Vogelsberger, M., Genel, S., Sijacki, D., et al. 2013, arXiv:1305.2913
Walter, F., Decarli, R., Carilli, C., et al. 2012, ApJ, 752, 93
Walter, F., Riechers, D., Cox, P., et al. 2009, Natur, 457, 699
Wang, R., Wagg, J., Carilli, C. L., et al. 2013, ApJ, 773, 44
Willott, C. J., Omont, A., & Bergeron, J. 2013, ApJ, 770, 13
Yajima, H., Li, Y., & Zhu, Q. 2012a, ApJ, 773, 151
Yajima, H., Umemura, M., & Mori, M. 2012b, MNRAS, 420, 3381
Yan, H., Dickinson, M., Stern, D., et al. 2005, ApJ, 634, 109
Young, J. S., Xie, S., Kenney, J. D. P., & Rice, W. L. 1989, ApJS, 70, 699